PAPER • OPEN ACCESS

Electric field effects on the dynamics of bubble detachment from an inclined surface

To cite this article: P Di Marco *et al* 2015 *J. Phys.: Conf. Ser.* **655** 012044

View the article online for updates and enhancements.

Electric field effects on the dynamics of bubble detachment from an inclined surface

P Di Marco[1]**, N Morganti, G Saccone**

DESTEC, University of Pisa, Largo Lucio Lazzarino 1, 56122, Pisa, Italy

Abstract. An experimental apparatus to study bubble detachment from an inclined surface under the action of electric forces is described. It consists of a container filled with FC72 at room temperature and pressure where a train of gas bubbles is injected from an orifice. An electrostatic field can be imposed around the bubble, while the cell can be tilted from 0 to 90°. It is possible to study interface growth with the aid of high-speed cinematography. Since the interface is asymmetrical, a mirror system allowed to acquire, in the same frame, two images at 90° of the bubble. Different inclinations, injection rates and voltages were tested in order to couple the effects of shear gravity and electric field. Curvature and contact angles have been derived with appropriate interpolation methods of the profile. Force balances on the bubble were checked, finding an electric force, which, at first pulls the bubbles from the orifice, then pushes it against the surface. The motion of the center of gravity confirms this behaviour. A power balance has been developed to determine the energy contributions, revealing that surface growth incorporates both the effects of inlet power and electric field.

1. Introduction

Bubble detachment under gravity force of different intensity and direction is encountered in many industrial applications, from electrical power plants based on Rankine - Hirn cycles to the two-phase thermal management for space purposes. In particular, the interest is to predict bubble departure diameter and frequency from a heated wall in order to achieve an increasingly reliable comprehension of two-phase heat transfer. In space applications, the need to reduce size and weight of all thermal management systems (power generation, electronics cooling, cabin temperature control, waste management, and regenerative fuel cells) suggests to replace current single-phase cooling systems with two-phase ones. In fact, this technique can lead to order-of-magnitude enhancement in heat transfer coefficients, giving the possibility to reduce sensibly heat exchangers surface, size and weight 0. Heat transfer performance can be further improved with the application of an electric field (EF); it is particularly in space applications that this technique shows its relevance. It has been assessed also in terrestrial gravity environment that the application of EF enhances boiling heat transfer coefficient [2], [3], [4], [5], [6]; but the most interesting aspect is the possibility to act as a replacement of gravity where it lacks [7], [8].

A relevant part of the current activities in boiling heat transfer research focuses on the influence of a shear flow on bubble detachment from a heated surface. In these conditions, the bubble is subjected to a shear force, deforming the interface from its axisymmetric shape. Studying force balances, different models of bubble detachment in shear flow have been developed [9], [10], [11]. In general, in these

---

[1]   Corresponding author: p.dimarco@ing.unipi.it

models simplifying approximations of the relevant parameters have been adopted, like a spherical or hemispherical bubble shape and a constant contact angle. The more complicated components of force balances are surface tension, drag and lift forces.

A situation similar to shear flow can be reproduced by tilting the detachment surface, in order to have a force component parallel to the surface, due to the buoyancy acting on the bubble. In these conditions, by injecting a controlled amount of gas from an orifice in the liquid, a static or slowly growing interface can be created, which can be more easily characterized and studied in controlled conditions. The results will help in clarifying the role of a transverse force on bubble detachment, and can be compared with existing models in order to check their validity. The experiment constitutes also a ground-based support to RUBI, an experiment developed by an ESA scientific team aimed to studying bubble detachment in microgravity under the action of different forces, which will be installed in the International Space Station in the near future. The contribution of the present work in RUBI experiment is the investigation of the coupled effects of transverse force and electric field on bubble departure. Once the shear effects modify the shape of the bubble, the electric field distribution is, in turn, altered and the way it acts over the bubble can promote or prevent bubble departure and successive trajectory. The present experiment is intended to shed light over the effect of electric field when the interface is modified by a shear force.
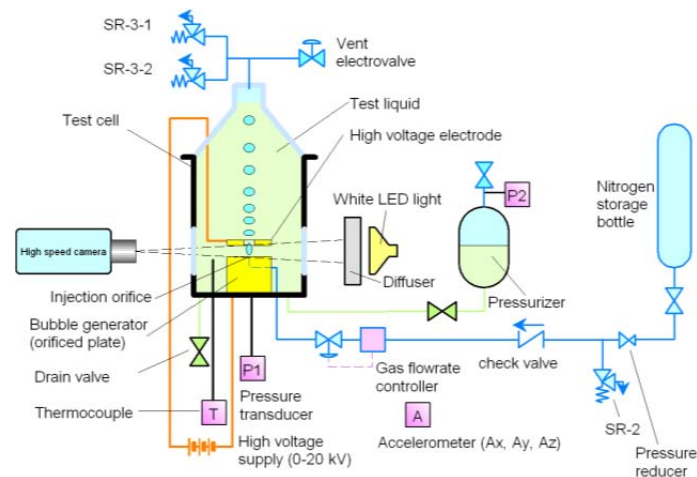
2. Experimental setup

The experimental setup used in the present work is the same one, which performed two parabolic flight campaigns carried out by ESA in 2013 and 2014. Its core (see Figure 1 and Figure 2) consists in a bubble generator, comprising a flat stainless steel plate with a circular orifice of 0.55 mm internal diameter drilled on it. The orifice was fed with nitrogen by means of a gas flowrate controller (Bronkhorst F-200, with a maximum flowrate of 100 mm^3/s). In this way, continuous trains of detaching bubbles, or individual bubbles growing very slowly can be generated. In the present experiments, the gas flowrate was limited to a maximum of 7 mm^3/s, in order to remain within the range of the so-called quasi-static detachment regime, where the detachment volume is independent of the gas flowrate, defined by the adimensional Tsuge parameter [12]:

$$\frac{\rho_l \, u_0 \, D_{or}^{1.5} \, g^{0.5}}{\sigma} = N_w < 1 \tag{1}$$

where ρ_l is the liquid density, u_0 is the gas velocity at the orifice and D_{or} the orifice diameter. The test cell (Figure 2) is an aluminum box (volume: about 0.7 L) filled with the test liquid (FC-72). The internal configuration of the cell makes it possible to orient the bubble generator both upwards and downwards. The cell is provided with four Lexan windows on its sides to allow high-speed image recording and illumination. The injected gas is collected in the upper cone of the test cell and, when the collected volume interferes with experiment operation, is vented through an electrovalve. To provide elasticity to the system, the cell is connected to an expansion volume (about 0.05 L) provided with an elastic membrane facing a gas volume where the pressure is controlled by venting and injection valves. The cell was operated at a pressure close to the atmospheric, approximately 100 kPa. The set of measurements is completed by a tri-axial accelerometer, a K-thermocouple for fluid temperature and an absolute pressure transducer.

An electric potential up to 25 kV dc could be applied to a washer-shaped electrode (10x4 mm, 1 mm thickness), located 6 mm above the plate and centered with the orifice axis. Images of the growing and detaching bubble were taken by means of a high-speed camera (Redlake MotionPro Y3) equipped with a microscopic lens allowing for a spatial resolution of 115 pixel/mm. A dedicated mirror system has been developed in order to acquire in the same frame two contemporary images of the interface from different points of view at 90° (see Figure 3a) in order to detect the asymmetries in bubble growth due to the component of gravity parallel to the surface. The acquisition of images in the same

frame avoided the necessity to synchronize frames acquired by different cameras, and made the data processing simpler. Various inclinations have been achieved by tilting the whole experimental rack and checking with the accelerometer when the inclination reached the desired value (see Figure 3b).

Figure 1: Sketch of the experimental apparatus.
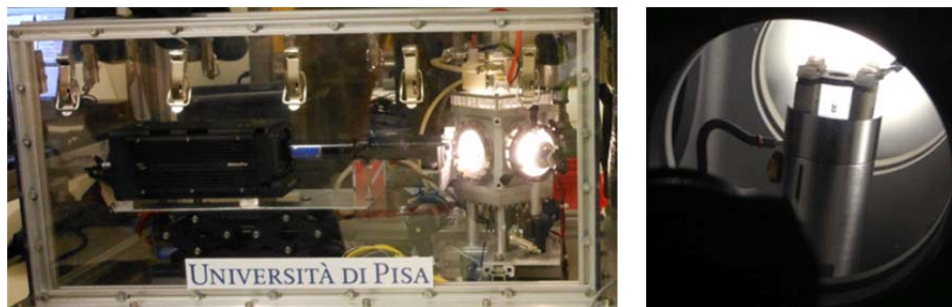
Figure 2: Photo of secondary containment assembled on the rack (left) and detail of the test cell (right) showing the orifice plate and the electrode inside the cell.
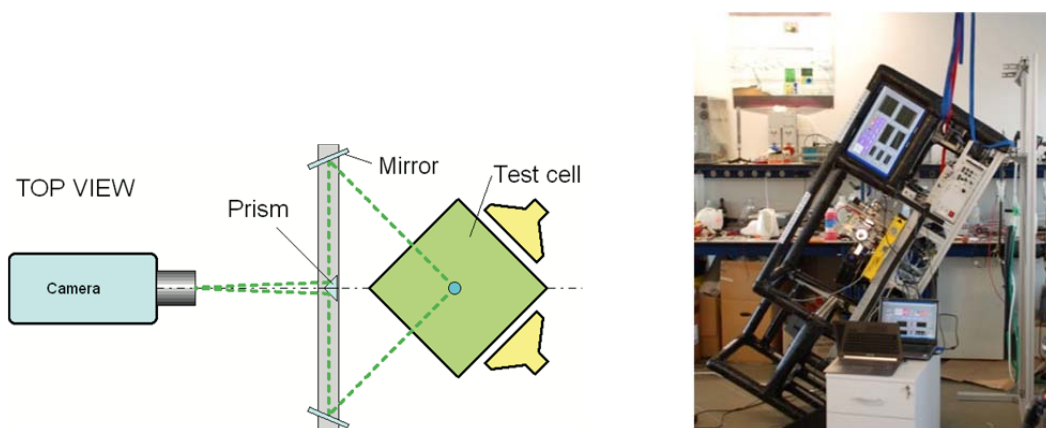
Figure 3: a) Optical arrangement (left). b) Inclination of the test section (right)

3. Force balances

The momentum balance in a control volume surrounding the bubble on the liquid side and the gas side of the base *A* reads (see Figure 4):

$$\frac{\mathrm{d}}{\mathrm{d}\,t}\int_V \rho_g \mathbf{v}\,\mathrm{d}V = \int_V \rho_g \mathbf{g}\,\mathrm{d}V + \int_S \left(\bar{\bar{\mathbf{T}}}_{v,f} - p_f \bar{\bar{\mathbf{I}}} + \rho \mathbf{v}_f(\mathbf{v}_f - \mathbf{v}_s) + \bar{\bar{\mathbf{T}}}_{e\,f}\right)\cdot \mathbf{n}\ \mathrm{d}S +$$

$$+ \int_A \left(\bar{\bar{\mathbf{T}}}_{v,g} - p_g \bar{\bar{\mathbf{I}}} + \rho \mathbf{v}_g(\mathbf{v}_g - \mathbf{v}_s) + \bar{\bar{\mathbf{T}}}_{eg}\right)\cdot \mathbf{n}\ \mathrm{d}S + \int_{CL} \sigma_{fg}\mathbf{t}_{fg}\,\mathrm{d}L = 0 \qquad (2)$$

Where, in particular, n and $\underline{t}$ are the normal outward and tangent (in the meridian plane) unit vectors, respectively, p is the pressure, v is the velocity, g is the gravity acceleration, $\bar{\bar{\mathbf{T}}}_e$ is the Maxwell stress tensor, $\bar{\bar{\mathbf{T}}}_v$ is the viscous stress tensor, σ is the surface tension (directed along t, tangent to bubble surface at contact line). The suffixes g, f are referred to gas and liquid sides, respectively. The inertial term in LHS is generally negligible, as only the inertia of the gas is must be taken into account here. Dynamical effects (including the surrounding liquid inertia) are accounted for in the normal and tangential stress distribution around the bubble, which must be evaluated taking into consideration the surrounding fluid motion.

Neglecting dynamical actions and interfacial mass transfer, integration of momentum equation gives a balance of buoyancy and excess of internal pressure, surface tension at the contact line and electric force:

$$\frac{\pi D_{or}^2}{4}\left[2\sigma\left(\frac{1}{R_1} + \frac{1}{R_2}\right) - \rho_f g L\right]\mathbf{j} - V_b(\rho_f - \rho_g)\,\mathbf{g}\ = \oint_{CL} \sigma \mathbf{t}_{fg}\,\mathrm{d}s + \int_S \bar{\bar{\mathbf{T}}}_{e,f}\cdot \mathbf{n}\ \mathrm{d}S \qquad (3)$$

Where R_1 and R_2 are the curvatures at bubble top, and the local value of contact angle θ has to be considered in the first term of RHS. Projecting the components along local coordinates x (parallel to the surface) and y (perpendicular to the surface), the expressions of vertical and tangential forces are obtained, as reported in Table 1. In particular, the surface tension term has been calculated assuming a linear trend (from β_{max} to β_{min}) of the contact angle versus the polar coordinate along the circumference of the orifice (see Figure 4b).

The force balance without electric field is verified first against the experimental data. Once it has been assessed, the electric contribution is calculated by algebraic sum of the other forces.

Table 1. Force components

	X component (tangential)	Y component (perpendicular)
Buoyancy	$V(\rho_f - \rho_g)g\sin\vartheta$	$V(\rho_f - \rho_g)g\cos\vartheta$
Pressure	none	$\frac{\pi D_{or}^2}{4}\left[2\sigma\left(\frac{1}{R_1} + \frac{1}{R_2}\right) - \rho_f g L\right]$
Surface tension	$\pi D_{or}\dfrac{\beta_{max} - \beta_{min}}{\pi^2 - (\beta_{max} - \beta_{min})^2}(\sin\beta_{max} - \sin\beta_{min})$	$\pi D_{or}\dfrac{\cos\beta_{max} - \cos\beta_{min}}{\beta_{max} - \beta_{min}}$
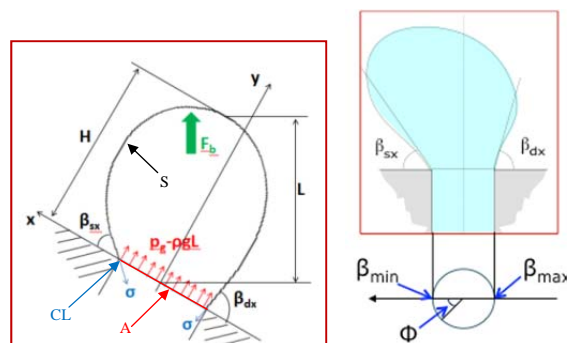
Figure 4: a) Control volume for force calculation. b) Contact angle variation vs. the polar coordinate.

4. Power balance

A last balance will be considered for completeness, i.e. the overall energy balance. It has been presented and ([13]) validated ([14] and [15]) for spreading droplets and has been adapted to study bubble evolution. The phenomena and their contribution to the change in the energy of the bubble are listed below.

- Inlet contribution; this term is mainly due to pressure developed by the injection system, the inlet velocity and by the pressure inside the bubble. It will be labelled as P_{inlet}.

$$P_{inlet} = \frac{dm}{dt}\left[\frac{p_{base} - p_{atm}}{\rho} + \frac{v_{inlet}^2}{2} \right] \tag{4}$$

- Surface potential energy; this term is very effective, it is due to the surface tension energy of the shape and depends on the interface area. It will be labelled as P_{surf}.

$$P_{surf} = \sigma \frac{dA_{fg}}{dt} \tag{5}$$

- Gravitational potential energy; this term is due to change of height of the center of gravity. It will be labelled as P_{grav}.

$$P_{grav} = g\left[m\frac{dz}{dt} + z\frac{dm}{dt} \right] \tag{6}$$

Finally, the overall energy balance in the absence of EF reads as follows:

$$P_{inlet} = P_{surf} + P_{grav} \tag{7}$$

5. Image processing and parameters calculation

The interface shape has been digitized with a dedicated image processing software, based on Matlab. The profile is identified from the grey-scale image by Canny method, with an imposed threshold. The geometrical parameters like curvature and apparent contact angles have been derived with appropriate interpolation methods of the profile [16]. In particular, for what concerns the curvature at the drop top, the 5 highest points are considered (see Figure 5a) and a 2nd order polynomial fitting is performed.
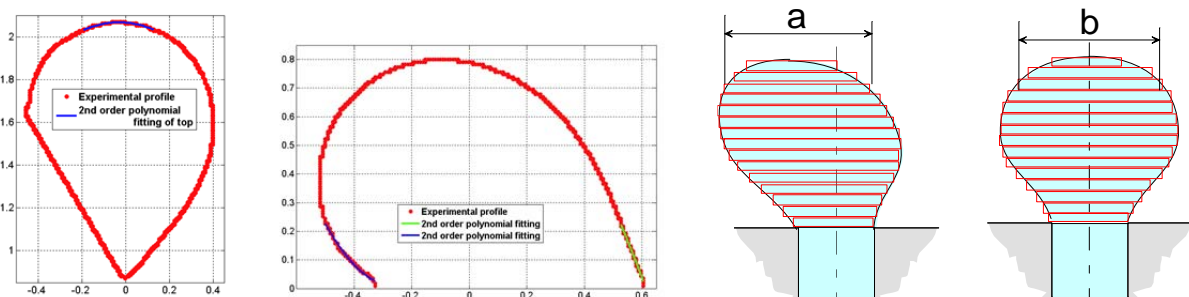
Figure 5: a) Curvature at top calculation. b) Contact angles calculation. c) Volume calculation as a stack of ellipses 1 pixel height; *a* is the major, *b* the minor axis.

When the electric field is not applied, the curvature at bubble top was calculated fitting the highest (in the direction of gravity) points. When the electric field was applied, bubble top turned to be the farthest point in the direction perpendicular to the surface. This is because electric field creates a

pressure contribution inside the droplet, which does not follow the gravity field, but the gradient of the electric potential [8], [17].

The polynomial fitting of contact angles was performed choosing the 25 lowest pixels (see Figure 5b). The bubble volume is determined considering the bubble as a stack of superposed ellipsoidal disks, of 1 pixel height, whose axes are the bubble widths in the two images (see Figure 5c) Once the geometrical parameters of the bubble are known, it was also possible determine the forces acting on it and to check the overall force balance on the inclined bubble.

6. Experimental uncertainty

The two most relevant variables affecting errors in the image processing technique described above are: the pixel size and the threshold chosen to identify the contour of the bubble. Pixel size has been determined *a priori* from the image recording of an object of sharp edges and known size. Error in the estimation of pixels and size of the objects are considered around 5% with a reference value of 115 pixel/mm. In the uncertainty evaluation, a value of 8% has been conservatively adopted in order to check the error induced by a difference of 10 pixel/mm. The threshold is a user-determined dimensionless parameter, discriminating black from white in a grey scale. It is necessary to detect the profile of an object in a grey scale image. The sharper is the contour of the image, the lower is the error induced by its choice. In the present study a nominal value of 0.8 has been chosen and a variation of ±0.05 has been considered. Since these sources of uncertainty are independent and the error distributions can be assumed Gaussian, the total uncertainty for the quantity φ is calculated as:

$$\sigma_\varphi = \sqrt{\left(\frac{\partial\varphi}{\partial ps}\Delta ps\right)^2 + \left(\frac{\partial\varphi}{\partial l}\Delta l\right)^2} \tag{8}$$

Uncertainty in the determination of linear parameters (i.e. bubble height) has been evaluated to be up to 8%, while volume uncertainty can rise to more than 20% for small bubbles. It is worth noting that the larger part of uncertainty is induced by the one in pixel size, and only a small amount is due to the threshold choice. One of the most relevant parameters in the present study is contact angle, whose uncertainty depends in a complex way by the above mentioned parameters. Therefore it has been evaluated with computer simulation, and its variation versus scaling factor and threshold is shown in Figure 6.
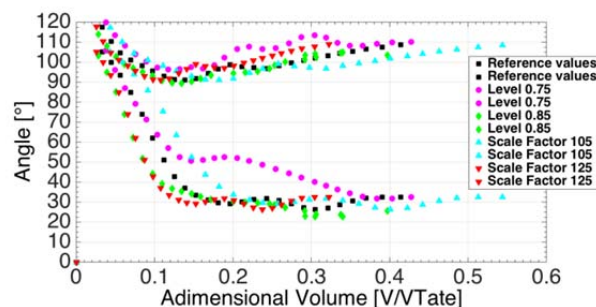
Figure 6: Contact angle variation with threshold (level) and pixel size (scale factor)

7. Results

Once the geometrical parameters of the bubble were known, it was possible to determine the forces acting on it and to check, the overall force balance on the inclined bubble. The overall force balance in vertical direction (inclinations 0 and 180°) has been already assessed and validated [18]. In the present work, different inclinations have been tested, with and without the electric contribution. For space limitations, the overall force balances in the tangential and perpendicular direction with respect to the

surface of 75° and 90° are shown comparing the behaviour of the two opposed case: 0kV and 25 kV. As already mentioned, once the force balance was verified in the absence of electric field, the electric force has been calculated as the algebraic sum of the other forces. The abscissa in following figures reports the bubble volume made non-dimensional by dividing by the so-called Tate's volume:

$$V_{Tate} = \frac{\pi D_{or} \sigma}{(\rho_f - \rho_g) g} \tag{9}$$

For what concerns the *x*-components, as remarked in Table 1, pressure force is absent, so the equilibrium is achieved by the *x*-components, of gravity and capillary (surface tension) forces. In the absence of electric field (see Figure 7) the resulting unbalance resultant lies below 2 μN, not far from the absolute uncertainty already obtained in previous experiments (1 μN in [18]), but since forces are much smaller, the relative error can grow up to 35% (worst case calculated).
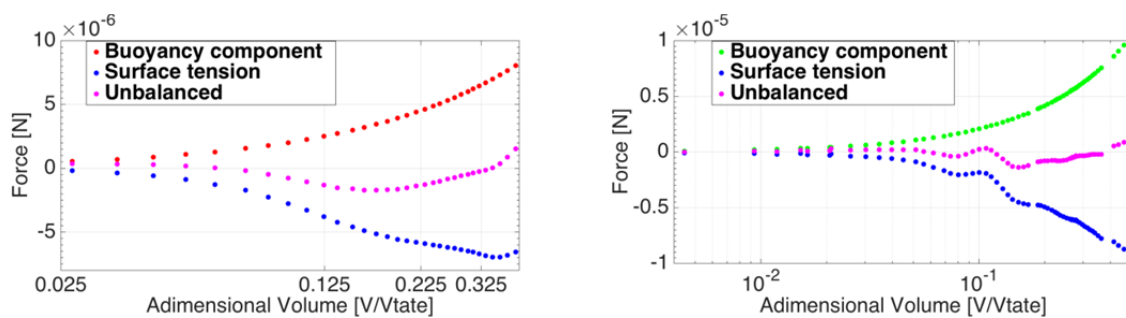
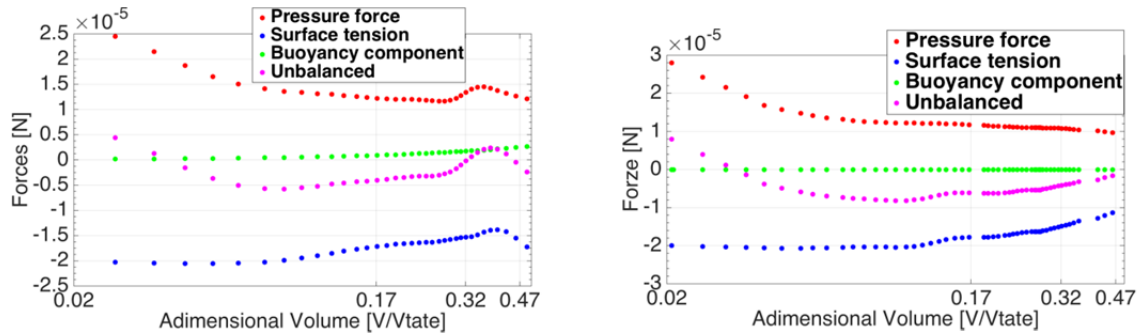**Figure 7**: Force balance, x direction, 75° (a) and 90° (b) of tilting, no EF.

After the application of electric field, a force opposing buoyancy can be noted (Figure 8). It seems that the electric field is pulling the bubble downwards, preventing asymmetries in bubble growth. The same behaviour has been assessed also for droplets immersed in an external electric field [13].
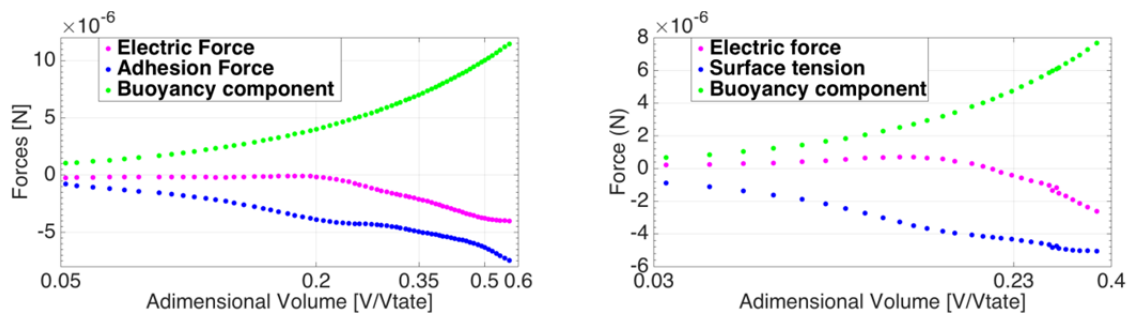
Figure 8: Force balance, *x* direction, 75° (a) and 90° (b) of tilting, with EF (25 kV).

Concerning the vertical direction, the case without electric field (Figure 9) reveals a lower error with respect to the balance in tangential direction, around 30% in the worst case.

Figure 9: Force balance, *y* direction, 75° (a) and 90° (b) of tilting, no EF.

The electric contribution (Figure 10) results to pull the bubbles away from the orifice. This lift component increases with the tilting angle.
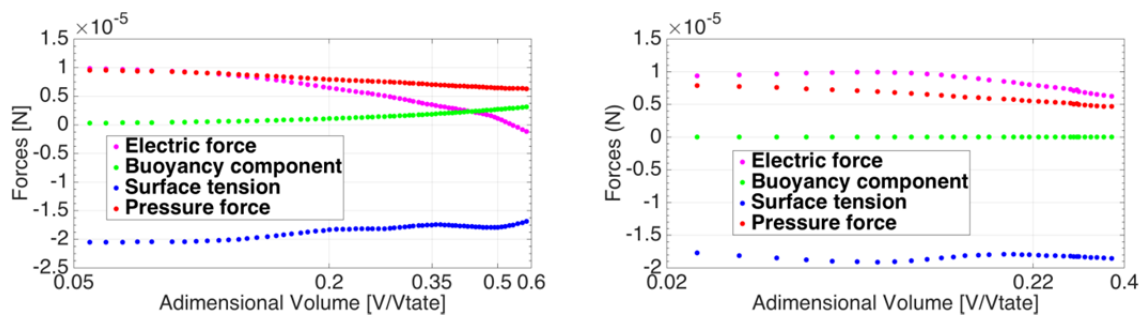

Figure 10: Force balance, *y* direction, 75° (a) and 90° (b) of tilting, with EF (25 kV).

Despite the electric contributions acting over the interface, the contact angle seems not to be altered substantially by the application of electric field until a certain volume value, as can be noticed comparing the history of contact angle for the 0kV and 25 kV cases at the same tilting condition, see Figure 11. This result has also been found in normal gravity and for 180° of tilting in [18].

The motion of the centre of mass of the bubble agrees with the presented force balances. As shown in Figure 12, the electric field pulls the bubble from the orifice towards the electrode and then, close to detachment and after, it pushes the bubble towards the surface.
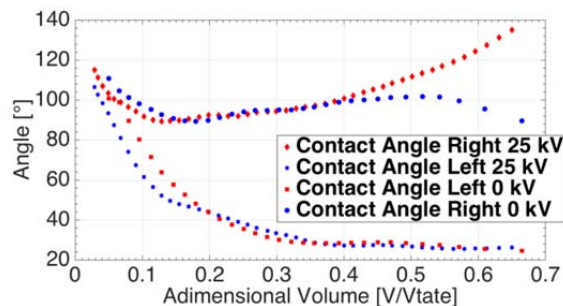

Figure 11: Contact angle, 0kV vs 25kV at 75°
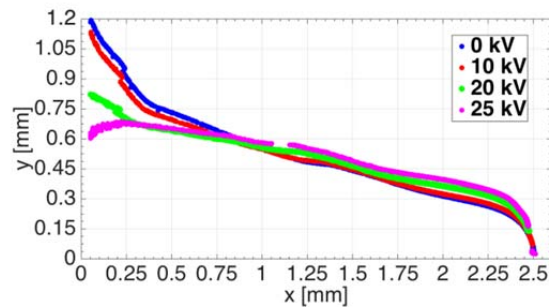
Figure 12: Motion of the centre of mass in function of the applied voltage, 75° of tilting.

For the power balance, the same procedure has been adopted, validating the model first for bubbles (Figure 13) and then determining by difference the contribution of the electric field.
Without electric field, the power spent in the gravitational term is very low compared to the other contributions: surface growth is storing all energy due to pressure and inlet flux.
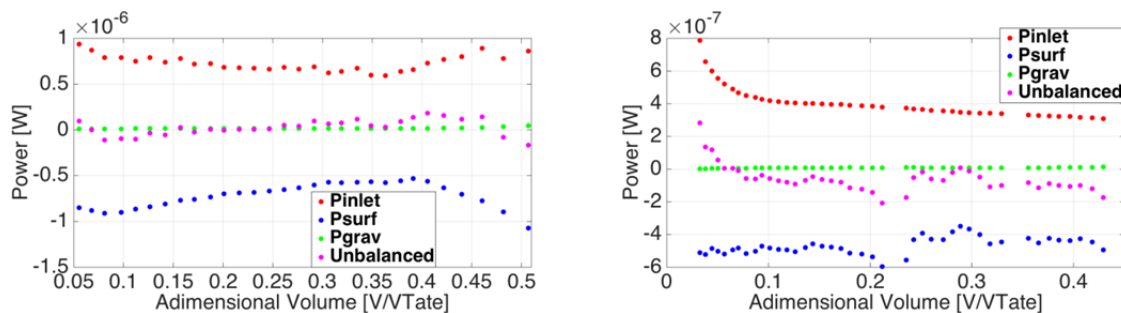
**Figure 13**: Power balance, 75° (a) and 90° (b) of tilting, no EF.

In the case of applied electric field, an interesting phenomenon can be noticed: in the case of bubbles, differently from droplets, the gravitational term in the power balance is positive (Figure 14). It means that the inlet power doesn't have to withstand it. This condition differs for droplets, where the inlet power is spent both in the growth of the interface and in the rise of the centre of gravity. The interest of this behaviour lies in the fact that when the electric field is applied, it follows the gravity one: for droplets the contribution of the electric field is negative, while for bubbles, the present work shows that it is positive. This is consistent with the fact that the creation of a cavity (with lower dielectric permittivity) causes a reduction of electrostatic energy in the domain. The energy recovered from gravitational and electric terms is used to create the bubble interface.
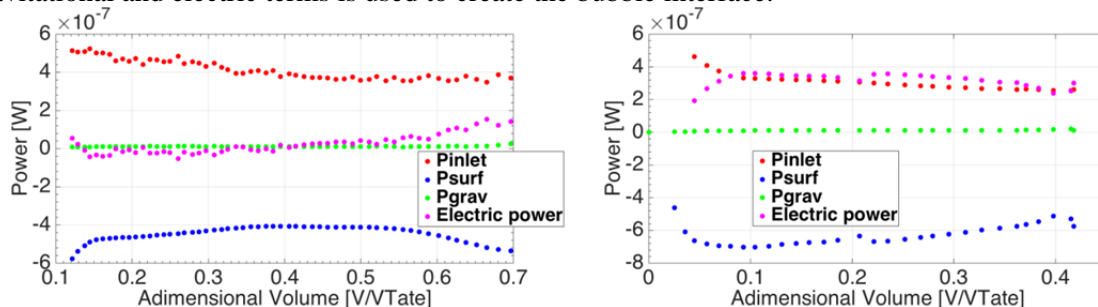
Figure 14: Power balance, 75° (a) and 90° (b) of tilting, with EF (25 kV).

A last figure summarizes all the effects just presented: in Figure 15, the detachment diameter in function of the tilting angle, for different electric potential applied is presented. As can be noticed, the detachment diameter decreases with increasing tilting angle, but it increases with increasing the electric field. In authors' opinion it can be due to the fact that electric forces are contributing in a

negative sense to the tangential-x force balance, thus reducing the effects of the shear component of gravity. This detachment diameter increase is negligible at the maximum tilting angle.
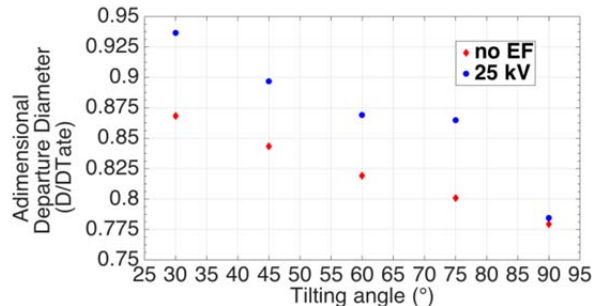
Figure 15: Detachment diameter as function of the tilting angle and of the electric field.

8. Conclusions

Bubbling of FC-72 at different tilting angle and different external electric potential applied has been studied experimentally to determine how tangential forces affect the shape and the behaviour of a single bubble, in order to understand the effect of electric field application to flow boiling.
In general it has been found that the electric field does not affect the contact angle of bubbles, but the resulting perpendicular force it is pulling the bubble away from the orifice during the growth and later, during and after detachment it pushes the bubble against the surface. In this way the bubble is forced to slide along the surface, which may significantly increase the boiling heat transfer coefficient.
Power balances reveal a further increase in the interface growth to compensate the negative electric contribution, thus promoting heat and mass transfer across the interface.
A possible drawback of the application of the electric field is the increase of departure diameter, due to the opposition of electric field to the shear force. In any case, this increase has been found to be very small for all the considered tilting angles (7.4% maximum) and to decrease with increasing tilting angle.

Acknowledgements

References

[1]   Zhang H, Mudawar I, Hasan M M 2008 *Thermal and Thermomechanical Phenomena in Electronic Systems ITHERM 11th Intersociety Conference* 949
[2]   Sharifi P 2011 *PhD Thesis, Southern Illinois University at Carbondale* UMI Number: 3460461
[3]   Zaghdoudi M C and Lallemand M 2005 *Arabian Journal for Science and Eng.* **30** 189
[4]   Di Marco P and Grassi W 1993 *J. Enhanced Heat Transfer* **1** 99
[5]   Bonjour E, Verdier J, Weil L 1962 *AIChE-ASME 5th Nat. Conference*
[6]   Allen P H G and Karayiannis T 1995 *Heat Recovery Systems & CHP* **5** 389
[7]   Di Marco P and Grassi W 2007 *Multiphase Sci. Technol.* **19 2** 141
[8]   Di Marco P, Kurimoto R, Saccone G, Hayashi K, Tomiyama A 2014 *Proc. 15th Int. Heat Transfer Conference* paper 8960 p 1
[9]   Duhar G and Colin C 2006 *Physics of Fluids* **18** 077101
[10] Klausner J F, Mei R, Bernhard M D, Zeng L Z 1993. *Int. J. Heat and Mass Tr.* **36** 651
[11] Thorncroft G E, Klausner J F, Mei R 2001 *Multiphase Science and Technology* **13** 35
[12] Tsuge H 1986 *Encyclopedia of Fluid Mechanics* chap. 9 191

[13] Erickson D, Blackmore B, Li D 2001 *Colloids and Surf. A: Physicochem. Eng. Aspects* **182** 109

[14] Saccone G, Del Seppia G, Rossi C A, Di Marco P 2015 *Proc. Droplet Impact Phenomena and Spray Investigation DIPSI Workshop*, University of Bergamo

[15] Saccone G 2014 *Master Thesis*, University of Pisa

[16] Di Marco P 2009 *7th W. Conf. on Exp. Heat Tr., Fluid Mech., Thermodynamics* 1

[17] Di Marco P and Saccone G, 2012 *23rd International Symposium on Transport Phenomena* 1

[18] Di Marco P, Giannini N, Saccone G 2012 *ECI 8th Int. Conf. on Boiling and Cond. Heat Tr.* 1